Journal of Applied Mathematics and Physics, 2025, 13(10), 3431-3449
https://www.scirp.org/journal/jamp
ISSN Online: 2327-4379
ISSN Print: 2327-4352

Higher-Order Solitions and Their Mixed Interactions for the (2 + 1)-Dimensional KdV Equation

Meiling Duan, Keke Chen*

College of Mathematics and Statistics, Jishou University, Jishou, China
Email: *2951231714@qq.com

How to cite this paper: Duan, M.L. and Chen, K.K. (2025) Higher-Order Solitions and Their Mixed Interactions for the (2 + 1)-Dimensional KdV Equation. *Journal of Applied Mathematics and Physics*, **13**, 3431-3449.
https://doi.org/10.4236/jamp.2025.1310195

Received: September 15, 2025
Accepted: October 27, 2025
Published: October 30, 2025

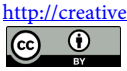

Abstract

In this paper, we primarily investigate several exact solutions of the (2 + 1)-dimensional KdV equation and summarize the trajectory equations after collisions between these solutions. Using the bilinear form with specific test functions and the parameter limiting technique, we construct T-order breather solutions, L-order lump solutions, and hybrid solutions. On this basis, we examine the close relationship between the positions of breather solutions and the parameters, the motion trajectories resulting from the interaction of lump solutions, as well as the trajectories of a single lump before and after its collision with higher-order soliton solutions.

Keywords

KdV-Equation, Bilinear Method, T-Order Breather Solutions, L-Order Lump Solutions, Hybrid Solutions, Collision Trajectories

1. Introduction

Nonlinear problems have grown in importance as modern physics, mechanics, and other natural sciences have advanced so quickly. Nonlinear partial differential equations (PDEs) or sets of PDEs can frequently be used to represent these nonlinear events in real-world applications. The study of exact solutions to nonlinear wave equations has continuously drawn a lot of attention, and solving differential equations is a long-standing research area with both theoretical and practical significance. The inverse scattering transform [1], *Darboux* transformation [2], *Bäcklund* transformation [3], bilinear method [4], symmetry reduction [5], the *Riemann-Hilbert* method [6]-[8], and the similarity transformation [9] are some of the established and potent techniques that have been developed to date.

Diederik Korteweg and Gustav de Vries, two Dutch mathematicians, first proposed the Korteweg-de Vries (KdV) equation in 1895 to explain the long-term asymptotic behavior of one-dimensional finite-amplitude waves. The KdV equation is an essential tool for comprehending nonlinear wave phenomena and holds a major place in the study of solitary waves, fluid dynamics, plasma physics, nonlinear optics, and mathematical research. The KdV equation is a significant research topic, and researchers have used a range of techniques to investigate its precise answers.

Gardner, *Greene*, *Kruskal*, *and Miura* linked the KdV equation to the linear *Schrdinger* equation, solving the nonlinear equation through scattering data [1]. Deift and Zhou combined the *Riemann-Hilbert* problem with the inverse scattering transform (IST) to obtain long-time asymptotic solutions [10]. Hirota derived the *N*-solition solutions of the (1 + 1)-dimensional KdV equation using the bilinear transformation [11]. Ma obtained lump solutions by extending the bilinear form [12]. Gandarias *et al.* derived power series solutions using the nonclassical symmetry reduction method [13]. Kudryashov employed the modified simple equation method to obtain exact solutions for the variable-coefficient KdV equation [14]. Wang *et al.* used the exponential function method to derive generalized solitary wave solutions [15]. In [16], Freeman and Nimmo introduced the *Wronskian* determinant method, constructing Wronskian-type solition solutions for the KP and KdV equations based on the bilinear method. In [17], Ma *et al.* derived complex-valued solutions of the KdV equation via the Darboux transformation. In [18], Ma and You applied the Wronskian determinant to solve the bilinear form of the KdV equation, using parameter transformation methods to construct rational solutions, solition solutions, and interaction solutions.

The exact solutions of the KdV equation bridge mathematical physics and real-world phenomena. In fluid dynamics, the KdV model mathematically describes Russell's "solitary wave" observations, with experiments confirming the elastic collision behavior of its multi-soliton solutions. In plasmas, the KdV single-soliton represents a localized positive potential pulse, forming an ion-acoustic density compression. In oceanography, it predicts internal wave propagation and its effects on marine structures. In nonlinear optics, the KdV principle of nonlinearity-dispersion balance underpins all soliton phenomena, accelerating the discovery of optical solitons and advancing long-distance fiber communications. From water waves to optical signals, the KdV equation reveals how order emerges from chaos across nature's domains.

While numerous scholars have studied various forms of exact solutions to the KdV equation, research on the mixed interactions of different solitions remains relatively scarce. Taking the following KdV system as an example, this paper investigates its exact solutions under specific transformations based on the bilinear form established in Reference [19].

$$\begin{cases} u_t + u_{xxx} + 3(uv)_x = 0 \\ u_x = v_y \end{cases} \tag{1}$$

The physical configurations and boundary conditions for variables u and v are typically determined by the specific physical phenomena being modeled. For instance, when searching for lump solutions or interacting soliton solutions, boundary conditions requiring decay to zero in both the x and y directions are commonly applied.

We perform the following transformation:

$$\begin{cases} u = u_0 + 2\left(\ln f\right)_{xy} \\ v = v_0 + 2\left(\ln f\right)_{xx} \end{cases} \tag{2}$$

where u and v are any seed solutions for the KdV equation. When specific seed solutions are chosen and incorporated into the transformation procedure, this enables us to obtain the corresponding bilinear formulation of the system.

The structure of this paper is organized as follows: In Section 2, we explore the positional relationships of higher-order breather solutions to the KdV equation under varying parameters. Section 3 and Section 4 utilize the long-wave limit method to derive higher-order lump solutions, as well as mixed solutions comprising lumps and higher-order solitons, along with trajectory equations following their interactions. Building upon our findings, Section 5 presents a comprehensive conclusion.

2. From *N*-Soliton to *L*-Order Breather Soliton

2.1. *N*-Soliton

Taking u_0 and v_0 as constants, the KdV equation transforms into its bilinear form:

$$\left(D_x^3 D_y + 3v_0 D_x D_y + 3u_0 D_x^2 + D_y D_t\right) f \cdot f = 0 \tag{3}$$

Within the bilinear formalism, the long-wave limit technique is applied to obtain the *N*-soliton solution for KdV equation in the following form:

$$f = f_N = \sum_{\nu=0,1} \exp\left(\sum_{i=1}^{N} \nu_i \zeta_i + \sum_{i<j}^{(N)} A_{ij} \nu_i \nu_j\right) \tag{4}$$

where the symbol $\sum_{\nu=0,1}$ represents the sum of combinatorial and permutational terms for $\nu_i = 0$ and $\nu_i = 1$, the $\sum_{i<j}^{(N)}$ represents the sum over all positive integers i satisfying $i < j$, and in the soliton solution of (4) must satisfy the condition:

$$\begin{cases} \zeta_i = k_i\left(x + \alpha_i y + \left(-k_i^2 - 3v_0 - \dfrac{3u_0}{\alpha_i}\right)t\right) + \sigma_i, \\ \mathrm{e}^{A_{ij}} = -\dfrac{\Psi_{ij}^{(1)} + \left(k_1\alpha_1 - k_2\alpha_2\right)\left(k_1\beta_1 - k_2\beta_2\right) + 3u_0\left(k_1 - k_2\right)^2 + 3v_0\left(k_1 - k_2\right)\left(k_1\alpha_1 - k_2\alpha_2\right)}{\Psi_{ij}^{(2)} + \left(k_1\alpha_1 + k_2\alpha_2\right)\left(k_1\beta_1 + k_2\beta_2\right) + 3u_0\left(k_1 + k_2\right)^2 + 3v_0\left(k_1 + k_2\right)\left(k_1\alpha_1 + k_2\alpha_2\right)}, \\ \Psi_{ij}^{(1)} = \left(k_1 - k_2\right)^3\left(k_1\alpha_1 - k_2\alpha_2\right), \\ \Psi_{ij}^{(2)} = \left(k_1 + k_2\right)^3\left(k_1\alpha_1 + k_2\alpha_2\right). \end{cases} \tag{5}$$

where $\alpha_i \neq 0$, and $k_i, \alpha_i, \beta_i, \sigma_i$ are some free parameters.

2.2. *L*-Order Breather Soliton

To obtain the L-th order breather solution, we need to impose conjugate parameter pairs in the N-soliton solution form while satisfying the following constraints:

$$N=2L, k_{i+1}=k_i^*, \alpha_{i+1}=\alpha_i^*, \beta_{i+1}=\beta_i^*, \sigma_{i+1}=\sigma_i^*, i=1,3,5,\cdots,2m-1 \tag{6}$$

Theorem 1 Based on bilinear Equation (3), the KdV Equation (1) has the following forms of 1-order breather solution

$$\begin{cases} v=v_0+2\dfrac{\left(a_{11}^2+a_{12}^2\right)^2 \iota-2a_{11}a_{12}\jmath+a_{11}^2M+a_{12}^2}{\iota^2} \\ u=u_0+2\dfrac{\left(\left(a_{11}^2+a_{12}^2\right)b_{11}\iota+\left(a_{11}^2-a_{12}^2\right)b_{12}+2a_{11}a_{12}b_{11}\right)\jmath}{\iota^2} \\ \quad +2\dfrac{Ma_{11}\left(a_{11}b_{11}-a_{12}b_{12}\right)+a_{12}\left(a_{11}b_{12}-a_{12}b_{11}\right)}{\iota^2} \\ \iota=\sqrt{M}\cosh\left(\iota_1+\ln\sqrt{M}\right)+\cos\left(\iota_2\right) \\ \jmath=\sqrt{M}\sinh\left(\iota_1+\ln\sqrt{M}\right)+\sin\left(\iota_2\right) \end{cases} \tag{7}$$

After simplification, we obtain

$$\tilde{f}_2=2\mathrm{e}^{\iota_1}\left(\sqrt{M}\cosh\left(\iota_1+\ln\sqrt{M}\right)+\cos\left(\iota_2\right)\right) \tag{8}$$

with

$$\begin{aligned} \iota_1&=a_{11}x+\left(a_{11}b_{11}-a_{12}b_{12}\right)y+\left(a_{11}c_{11}-a_{12}c_{12}\right)t+\sigma_0 \\ \iota_2&=a_{11}x+\left(a_{11}b_{12}+a_{12}b_{11}\right)y+\left(a_{11}c12+a_{12}c_{11}\right)t+\sigma_0 \end{aligned} \tag{9}$$

Substituting Equation (8) with Equation (9) in the KdV equation and performing the corresponding calculations yields 1-order breather solution. This completes the proof.

The first-order breather solution contains several undetermined parameters, where the quantitative relationships between these parameters can affect the position of the breather. In Figure 1, three positional configurations are illustrated, with all plots generated under the condition $t=0$. The parameters are specifically set as follows:

Figure 1(a): When $a_{11}=0$, $a_{11}b_{11}-a_{12}b_{12}\neq 0$, the breather is parallel to the x-axis, with parameter values: $k_2=k_1^*=\frac{2}{3}\mathrm{i}$, $\alpha_2=\alpha_1^*=\frac{1}{5}-\frac{1}{2}\mathrm{i}$, $\sigma_2=\sigma_1^*=0$.

Figure 1(b): When $a_{11}\neq 0$, $a_{11}b_{12}-a_{12}b_{12}\neq 0$, the breather is parallel to the $y=\dfrac{a_{11}}{a_{12}b_{12}-a_{11}b_{11}}$, with parameter values: $k_2=k_1^*=\frac{1}{4}-\frac{2}{3}\mathrm{i}$, $\alpha_2=\alpha_1^*=\frac{1}{3}-\frac{1}{2}\mathrm{i}$, $\sigma_2=\sigma_1^*=0$.

Figure 1(c): When $a_{11}\neq 0$, $a_{11}b_{11}-a_{12}b_{12}=0$, the breather is parallel to the y-axis, with parameter values: $k_2=k_1^*=\frac{14}{25}-\frac{12}{25}\mathrm{i}$, $\alpha_2=\alpha_1^*=\frac{12}{21}-\frac{14}{21}\mathrm{i}$, $\sigma_2=\sigma_1^*=0$.

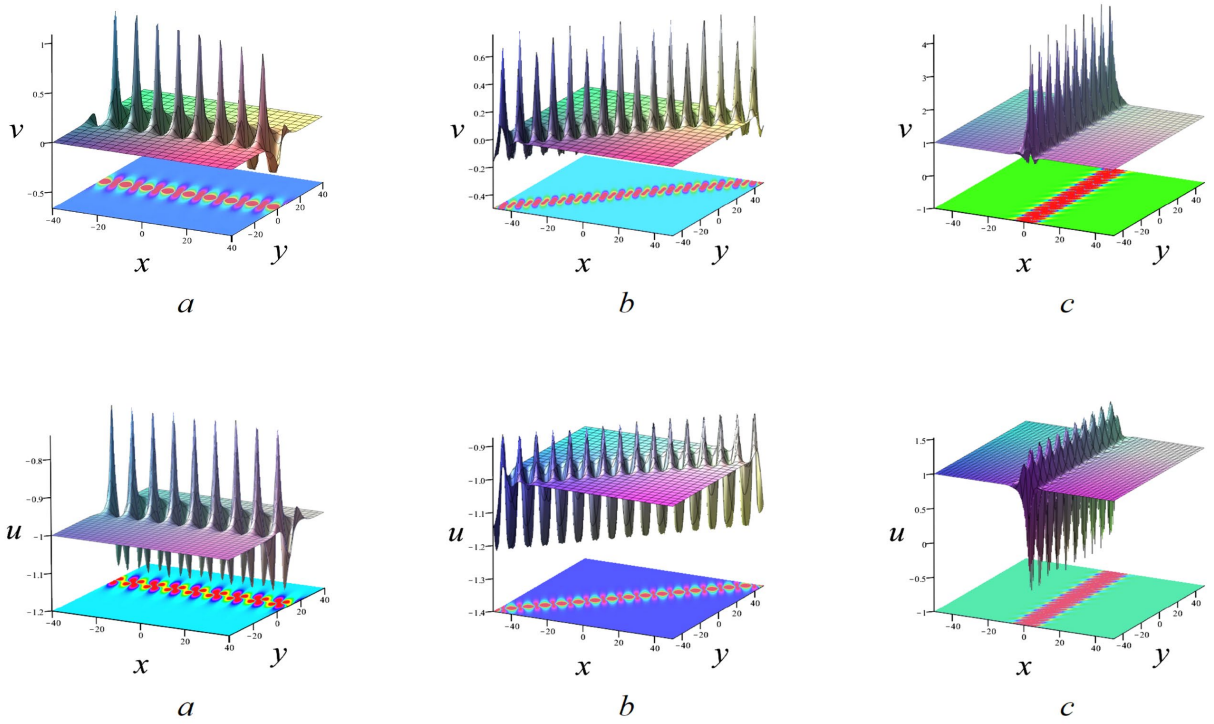

Figure 1. Spatial structure diagram of the 1st-order breather for the KdV equation at $t=0$: (a) Perpendicular to the *x*-axis; (b) With a slope of 1; (c) Perpendicular to the *y*-axis.

The 2th-order breather solution may be constructed with the conditions of $L=2$ and choose parameters as:

$$\begin{aligned} &k_2=k_1^*=a_{11}-a_{12}I, k_4=k_3^*=a_{21}-a_{22}I,\\ &\alpha_2=\alpha_1^*=b_{11}-b_{12}I, \alpha_4=\alpha_3^*=b_{21}-b_{22}I,\\ &\beta_2=\beta_1^*=c_{11}-c_{12}I, \beta_4=\beta_3^*=c_{21}-c_{22}I,\\ &\sigma_2=\sigma_1^*, \sigma_4=\sigma_3^* \end{aligned} \tag{10}$$

Figure 2 illustrates the spatial structures of three distinct second-order breather solutions, which depend on the relationships between the parameters. Four positional configurations are illustrated, with all plots generated under the condition $t=0$. The parameters are specifically set as follows:

Figure 2(a): Under the condition that $a_{i1}=0$, $a_{i1}b_{i1}-a_{i2}b_{i2}\neq 0$, $(i=1,2)$ is satisfied, by selecting specific parameters as: $k_2=k_1^*=\frac{6}{5}\mathrm{i}$, $k_4=k_3^*=\frac{4}{3}\mathrm{i}$, $\alpha_2=\alpha_1^*=\frac{2}{7}-\frac{13}{4}\mathrm{i}$, $\sigma_i=0(i=1,2,3,4)$, $t=5$, we can obtain a 2-order breather solution parallel to the x-axis.

Figure 2(b): Under the condition that $a_{i1}\neq 0$, $a_{i1}b_{i1}-a_{i2}b_{i2}=0$, $(i=1,2)$ is satisfied, by selecting specific parameters as: $k_2=k_1^*=1-\frac{4}{12}\mathrm{i}$, $k_4=k_3^*=\frac{7}{9}+\frac{4}{6}\mathrm{i}$, $\alpha_2=\alpha_1^*=\frac{2}{6}-1\mathrm{i}$, $\alpha_4=\alpha_3^*=\frac{4}{6}-\frac{7}{9}\mathrm{i}$, $\sigma_i=0(i=1,2,3,4)$, $t=0$, we can obtain a two-breather solution parallel to the y-axis.

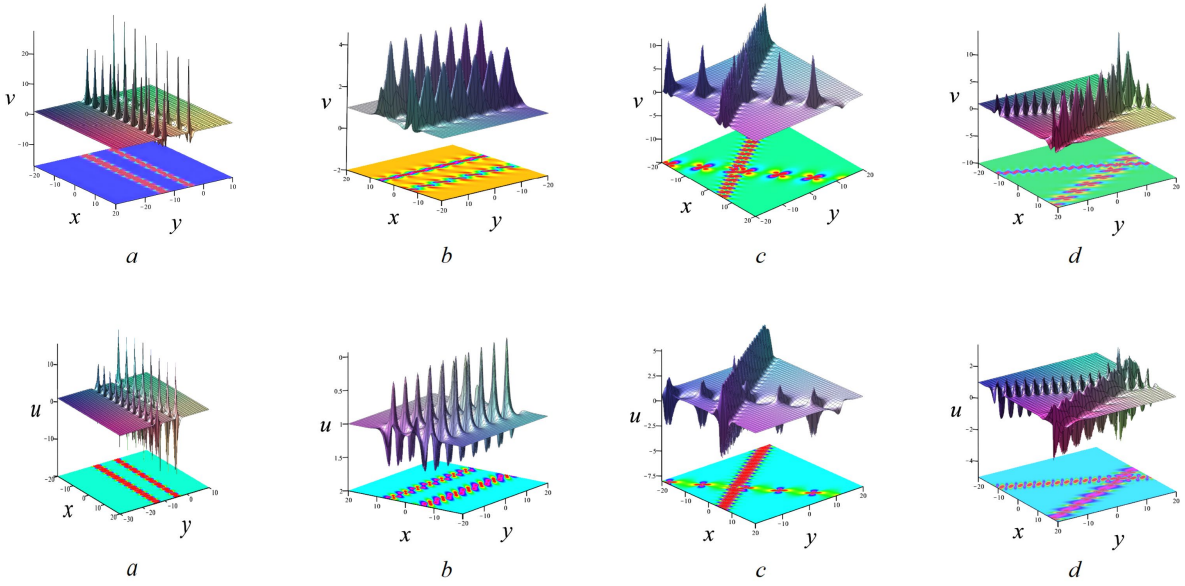

Figure 2. Spatial structure diagram of the 2nd-order breather for the KdV equation at $t=0$: (a) (b) Parallel to each other; (c) Mutually perpendicular; (d) Intersect with each other.

Figure 2(c): Under the condition that $a_{12}\left(a_{11}b_{11}-a_{12}b_{12}\right)+a_{11}\left(a_{21}b_{21}-a_{22}b_{22}\right)=-1$ is satisfied, by selecting specific parameters as: $k_2=k_1^*=\frac{1}{2}-\frac{2}{3}\mathrm{i}$, $k_4=k_3^*=1+\frac{3}{2}\mathrm{i}$, $\alpha_2=\alpha_1^*=\frac{3}{2}\cdot\mathrm{i}$, $\alpha_4=\alpha_3^*=-\frac{5}{6}-1\mathrm{i}$, $\sigma_i=0\left(i=1,2,3,4\right)$, $t=0$, the structure diagram of a vertically oriented 2-order breather can be obtained.

Figure 2(d): Under the condition that $a_{12}\left(a_{11}b_{11}-a_{12}b_{12}\right)+a_{11}\left(a_{21}b_{21}-a_{22}b_{22}\right)\neq 0$ is satisfied, by selecting specific parameters as: $k_2=k_1^*=1-\frac{2}{3}\mathrm{i}$, $k_4=k_3^*=1+\frac{3}{2}\mathrm{i}$, $\alpha_2=\alpha_1^*=\frac{2}{6}-\frac{1}{2}\mathrm{i}$, $\alpha_4=\alpha_3^*=\frac{5}{6}-1\mathrm{i}$, $\sigma_i=0\left(i=1,2,3,4\right)$, $t=1$, the structural diagram of the second-order breather with interaction at a certain angle can be obtained.

The 3-order breather solution may be readily constructed with the conditions of $N=6, L=3$ and choosing parameters as

$$\begin{aligned}&k_2=k_1^*=a_{11}-a_{12}I, k_4=k_3^*=a_{21}-a_{22}I, k_6=k_5^*=a_{31}-a_{32}I\\&\alpha_2=\alpha_1^*=b_{11}-b_{12}I, \alpha_4=\alpha_3^*=b_{21}-b_{22}I, \alpha_6=\alpha_5^*=b_{31}-b_{32}I\\&\beta_2=\beta_1^*=c_{11}-c_{12}I, \beta_4=\beta_3^*=c_{21}-c_{22}I, \beta_6=\beta_5^*=c_{31}-c_{32}I\\&\sigma_2=\sigma_1^*, \sigma_4=\sigma_3^*, \sigma_6=\sigma_5^*\end{aligned} \tag{11}$$

Figure 3 illustrates the spatial structures of three distinct second-order breather solutions, which depend on the relationships between the parameters:

Figure 3(a): Under the condition that $a_{i1}=0$, $a_{i1}b_{i1}-a_{i2}b_{i2}\neq 0\ \left(i=1,2,3\right)$ is satisfied, by selecting specific parameters as: $k_2=k_1^*=\frac{2}{5}-\frac{3}{5}\mathrm{i}$, $k_4=k_3^*=\frac{2}{5}-\frac{8}{9}\mathrm{i}$, $k_6=k_5^*=\frac{3}{7}-\frac{5}{8}\mathrm{i}$, $\alpha_2=\alpha_1^*=-\mathrm{i}$, $\alpha_4=\alpha_3^*=\mathrm{i}$, $\alpha_6=\alpha_5^*=\mathrm{i}$, $\sigma_i=0\left(i=1,\cdots,6\right)$,

$t=0$, we can obtain a 3-breath solution parallel to the x-axis.

Figure 3(b): Under the condition that $a_{i1}\neq 0$, $a_{i1}b_{i1}-a_{i2}b_{i2}=0\ (i=1,2,3)$ is satisfied, by selecting specific parameters as: $k_2=k_1^*=\frac{2}{2}-\frac{2}{2}\mathrm{i}$, $k_4=k_3^*=\frac{4}{5}+\frac{2}{7}\mathrm{i}$, $k_6=k_5^*=1+\frac{1}{7}\mathrm{i}$, $\alpha_2=\alpha_1^*=\frac{2}{4}-\frac{1}{2}\mathrm{i}$, $\alpha_4=\alpha_3^*=-\frac{2}{7}-\frac{4}{5}\mathrm{i}$, $\alpha_6=\alpha_5^*=\frac{1}{7}-1\mathrm{i}$, $\sigma_i=0(i=1,\cdots,6)$, $t=-2$, we can obtain a 3-breather solution parallel to the y-axis.

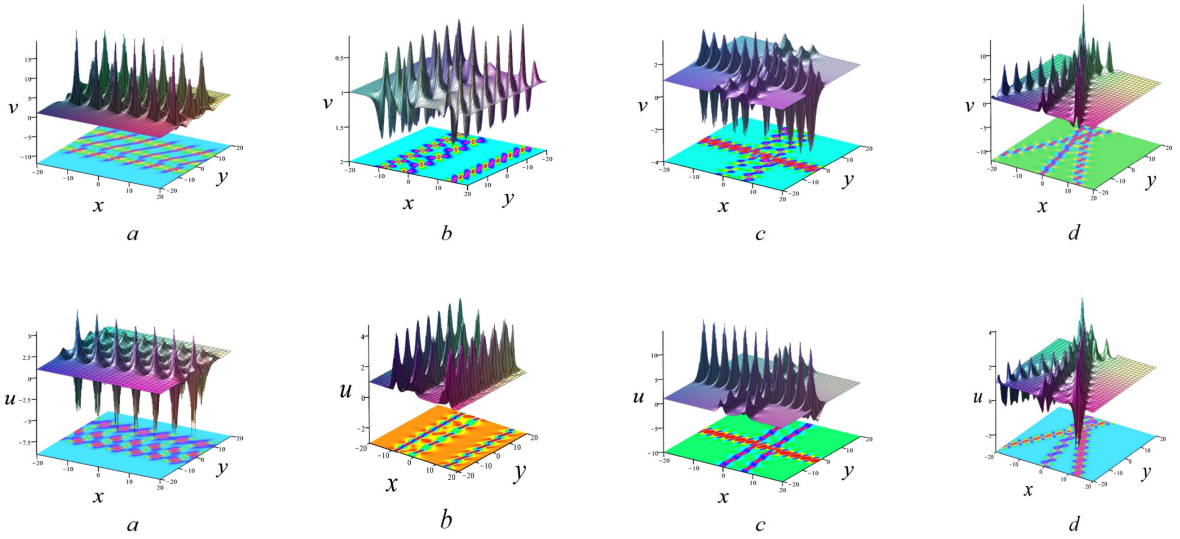

Figure 3. Spatial structure diagram of the 3rd-order breather for the KdV equation at $t=0$: (a) (b) Parallel to each other; (c) Mutually perpendicular; (d) Intersect with each other.

Figure 3(c): Under the condition that $a_{i1}=0$, $a_{i1}b_{i1}-a_{i2}b_{i2}\neq 0\ (i=2,3)$ is satisfied, by selecting specific parameters as: $k_2=k_1^*=\frac{8}{7}\mathrm{i}$, $k_4=k_3^*=1+\frac{1}{5}\mathrm{i}$, $k_6=k_5^*=1+\frac{1}{7}\mathrm{i}$, $\alpha_2=\alpha_1^*=-\frac{1}{4}-\frac{1}{2}\mathrm{i}$, $\alpha_4=\alpha_3^*=-\frac{1}{5}-1\mathrm{i}$, $\alpha_6=\alpha_5^*=-\frac{1}{7}-1\mathrm{i}$, $\sigma_i=0(i=1,\cdots,6)$, $t=0$, obtain a 3-breather structure composed of two parallel y-axis first-order breathers perpendicular to another x-axis parallel breather.

Figure 3(d): Under the condition that $a_{i1}\neq 0$, $a_{i1}b_{i1}-a_{i2}b_{i2}\neq 0\ (i=1,2,3)$ is satisfied, by selecting specific parameters as: $k_2=k_1^*=-1-\frac{2}{3}\mathrm{i}$, $k_4=k_3^*=1+\frac{3}{4}\mathrm{i}$, $k_6=k_5^*=1+\frac{1}{3}\mathrm{i}$, $\alpha_2=\alpha_1^*=-\frac{1}{4}-\frac{1}{2}\mathrm{i}$, $\alpha_4=\alpha_3^*=-\frac{1}{5}-1\mathrm{i}$, $\alpha_6=\alpha_5^*=-\frac{1}{7}-1\mathrm{i}$, $\sigma_i=0(i=1,\cdots,6)$, $t=-2$, obtain a 3-order breather formed by the intersection of three 1-order breathers.

The spatial structure and parameters of the T-th order breathing solutions are closely related, as discussed in previous sections 1-, 2-, and 3-order breather solition. Firstly, an T-th order breathing solution is composed of T breathing modes and the periodicity following the interaction of breathing modes remains

unchanged in terms of spatial structure. The position of each breathing mode in the (x,y) plane is associated with $y_i = \dfrac{a_{i1}}{a_{i2}b_{i2} - a_{i1}b_{i1}}$. When $y_1 = y_2 = \cdots = y_i$, the breathing modes are parallel; when $y_1 = y_2 = \cdots = y_i = 0$, they align parallel to the coordinate axes. Conversely, when $y_j \neq y_i, (i \neq j)$, the breathing modes intersect with each other. Furthermore, if $y_j y_i = -1, (i \neq j)$ exists within this framework, a perpendicular state emerges.

3. From *N*-Solution to *L*-Order Lump Solution and Trajectory Equations

This subsection focuses on investigating Lth-order lump solutions for the KdV equation. Building upon $\sigma_i = I\pi$, we employ the long-wave limit method by setting $k_i/k_j = o(1)$ while letting k_i approach zero, thereby obtaining the corresponding Lth-order rational solutions.

$$f_N = \prod_{i=1}^{N} \delta_i + \frac{1}{2}\sum_{i,j}^{N} P_{ij} \prod_{s\neq i,j}^{N} \delta_s + \cdots + \frac{1}{M!2^M} \sum_{i,j\cdots,m,n}^{N} \overbrace{P_{ij}P_{kl}\cdots P_{mn}} \prod_{q\neq i,j,k,l,\cdots,m,n}^{N} \delta_q + \cdots \quad (12)$$

with

$$\delta_i = x + \alpha_i y + \left(-3v_0 - \frac{3u_0}{\alpha_i}\right)t, \ P_{ij} = \frac{2\alpha_i\alpha_j(\alpha_i + \alpha_j)}{u_0(\alpha_i - \alpha_j)^2} \quad (13)$$

where, $\sum_{i,j,\cdots,m,n}^{N}$ represents the summation over all permutations of $i, j, \cdots, m, n$, where they can be positive integers within N. To obtain L-th order lump solution of the KdV equation in the above expression, it suffices to take the parameter α as follows: $\alpha_{L+i} = \alpha_i^* (1,2,\cdots,L)$, $N = 2L$ and $P_{i,j} > 0$. The symbol "$*$" denotes the complex conjugate.

Theorem 2 The KdV Equation (1) has the following forms of 1-order lump solution,

$$\begin{cases} u = u_0 + 4\dfrac{a_{11}(\theta^2 + \eta^2 + \Delta) - 2\theta(a_{11}\theta + a_{12}\eta)}{(\theta^2 + \eta^2 + \Delta)^2} \\ v = v_0 + 4\dfrac{1 - \theta^2}{(\theta^2 + \eta^2 + \Delta)^2} \end{cases} \quad (14)$$

Furthermore, we obtain the motion trajectory and velocity of the 1-order lump solution as:

$$y = -\frac{u_0 x}{\alpha_1\alpha_2 v_0 + \alpha_1 u_0 + \alpha_2 u_0} \quad (15)$$

$$v = \sqrt{\left(\frac{3t(\alpha_1\alpha_2 v_0 + \alpha_1 u_0 + \alpha_2 u_0)}{\alpha_1\alpha_2}\right)^2 + \left(-\frac{3tu_0}{\alpha_1\alpha_2}\right)^2} \quad (16)$$

Poof In the N solution (4), taking $N = 2$, $L = 1$, the rational solution f_2 can be expressed as

$$f_2 = \delta_1\delta_2 + P_{12},\ P_{12} = \frac{2\alpha_1\alpha_2(\alpha_1+\alpha_2)}{u_0(\alpha_1-\alpha_2)^2} \tag{17}$$

where $\delta_i = x + \alpha_i y + \left(-3v_0 - \frac{3u_0}{\alpha_i}\right)t$, $(i=1,2)$. In order to generate 1-lump solutions, we take $\alpha_2 = \alpha_1^* = a_{11} - a_{12}I$, the f_2 convert to

$$\begin{aligned} f_2 &= \left(x + a_{11}y + \left(-3v_0 - \frac{3u_0^2 a_{11}}{a_{11}^2 + a_{12}^2}\right)\right) \\ &\quad + \left(x + a_{12}y + \left(-3v_0 - \frac{3u_0^2 a_{12}}{a_{11}^2 + a_{12}^2}\right)\right) - \frac{a_{11}\left(a_{11}^2 + a_{12}^2\right)}{u_0 a_{12}^2} \\ &= \theta^2 + \eta^2 + \Delta \end{aligned} \tag{18}$$

Substituting (18) into (2), we obtain 1-order lump solution. Next, we prove the second part of the theory. According to the previous proof, we can obtain:

$$v = v_0 + 2(\ln f)_{xx} \tag{19}$$

Let $v_x = 0$, $v_y = 0$ in (19) and apply the extreme value theorem of binary functions, we can get the crest of the 1-order lump solution of (19).

$$x = \frac{3t(q_1q_2v_0 + q_1u_0 + q_2u_0)}{q_1q_2},\ y = -\frac{3tu_0}{q_1q_2} \tag{20}$$

Combining these two equations, we can derive the trajectory Equation (15). For the 1-lump solution, its velocity can be orthogonally decomposed into the components along the *x* and *y*-axes, denoted as v_x and v_y, respectively. By $v = \sqrt{v_x^2 + v_y^2}$, we can obtain the motion velocity (16). The theorem is thus proved.

In Figure 4, we select parameter $v_0 = 1$, $u_0 = -1$, $a_{11} = \frac{1}{3}$, $a_{12} = -\frac{1}{2}$, to illustrate the spatial profiles of the first-order lump solution at different time instances. Substituting the parameter into (15), we obtain the trajectory equation $y = -\frac{36x}{11}$. Three distinct colors are used to represent the states of the first-order rogue wave solution at three different times (see Figure 7(d1)).

When $N = 4, L = 2$, and $e^{\sigma_i} = -1, (i = 1,2,3,4)$ in (12), f_4 can be explicitly expressed as:

$$\begin{aligned} f_4 &= \delta_1\delta_2\delta_3\delta_4 + P_{12}\delta_3\delta_4 + P_{13}\delta_2\delta_4 + P_{14}\delta_2\delta_3 + P_{23}\delta_1\delta_2 + P_{24}\delta_1\delta_3 \\ &\quad + P_{23}\delta_1\delta_2 + P_{12}p_{34} + P_{13}p_{24} + P_{14}p_{23} \end{aligned} \tag{21}$$

where $\delta_i = x + \alpha_i y + \left(-3v_0 - \frac{3u_0}{\alpha_i}\right)t$, $P_{ij} = \frac{2\alpha_i\alpha_j(\alpha_i-\alpha_j)}{u_0(\alpha_i+\alpha_j)^2}$, $1 \le i < j \le 4$. By taking $\alpha_2 = \alpha_1^* = a_{11} - a_{12}I$, $\alpha_4 = \alpha_3^* = a_{21} - a_{22}I$ into (21), through simplification, the second-order lump solution can be obtained. Figure 5 shows the spatial structure diagrams of 2-order lump solution at different time points, with the selected parameters specifically being $v_0 = 1$, $u_0 = 1$, $a_{11} = \frac{1}{2}$, $a_{12} = \frac{3}{4}$, $a_{21} = -\frac{1}{5}$,

$a_{22}=-\frac{5}{6}$, When a 1-lump wave collides with other lump waves, its trajectory remains unchanged. By analogy with the solving process of the 1-order lump trajectory equation discussed earlier, we derive the motion trajectories of the 2-lump solutions as $y=-\frac{16x}{29}$ (black), $y=-\frac{900x}{301}$ (blue), respectively (see Figure 7(d2)).

When $N=6, L=3$ and $\mathrm{e}^{\sigma_i}=-1, (i=1,2,3,4,5,6)$, in (12), we can obtain f_6. By taking $\alpha_2=\alpha_1^*=a_{11}-a_{12}I$, $\alpha_4=\alpha_3^*=a_{21}-a_{22}I$, $\alpha_6=\alpha_5^*=a_{31}-a_{32}$ into f_6, after simplification, the 3-order lump soliton can be obtained. Figure 6 shows the spatial structure diagrams of 3-order lump solution at different time points, with the selected parameters specifically set as $v_0=1$, $u_0=1$, $a_{11}=\frac{1}{4}$, $a_{12}=\frac{2}{5}$, $a_{13}=-\frac{1}{5}$, $a_{21}=\frac{1}{2}$, $a_{22}=-\frac{2}{3}$, $a_{32}=-\frac{1}{2}$ (see Figures 6(a)-(c)). The 3D structures and collision trajectories of the 1-, 2-, and 3-lump solutions visually demonstrate how multi-lump interactions concentrate energy into a single lump at $t=0$, followed by post-collision dispersion into multiple lumps. The absence of phase shift confirms that the trajectory equations remain unchanged before and after collision. When a 1-lump wave collides with other lump waves, its trajectory remains unchanged. Similar to the analysis of 1st- and 2nd-order lump trajectories, we can derive the motion trajectories for 3rd-order lumps as follows: $y=-\frac{16x}{13}$ (red), $y=-\frac{225x}{316}$ (blue), $y=\frac{100x}{11}$ (green), respectively (see Figure 7(d3)). Furthermore, when $N=2L$, taking we can obtain the L-order lump solution of KdV equation. We can predict the situation of L-order lump solutions regarding spatial structure and motion trajectory equations.

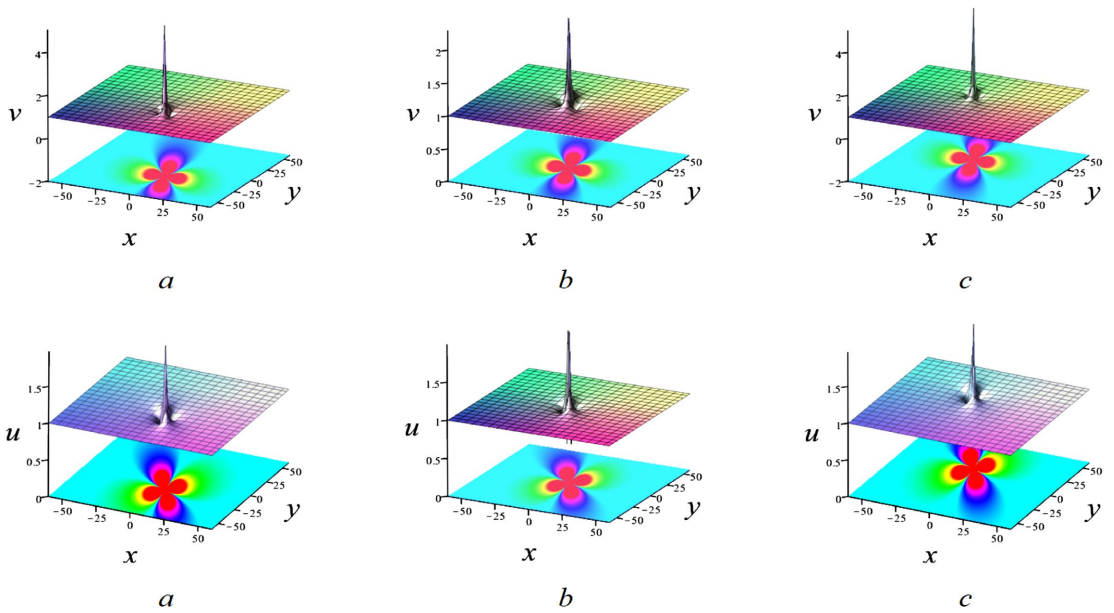

Figure 4. Patial structure diagram of the 1-order lump solution for the KdV equation along with the corresponding projection density plot, (a) - (c) show the spatial profiles of the lump solution in $t=2$, $t=0$, $t=-2$.

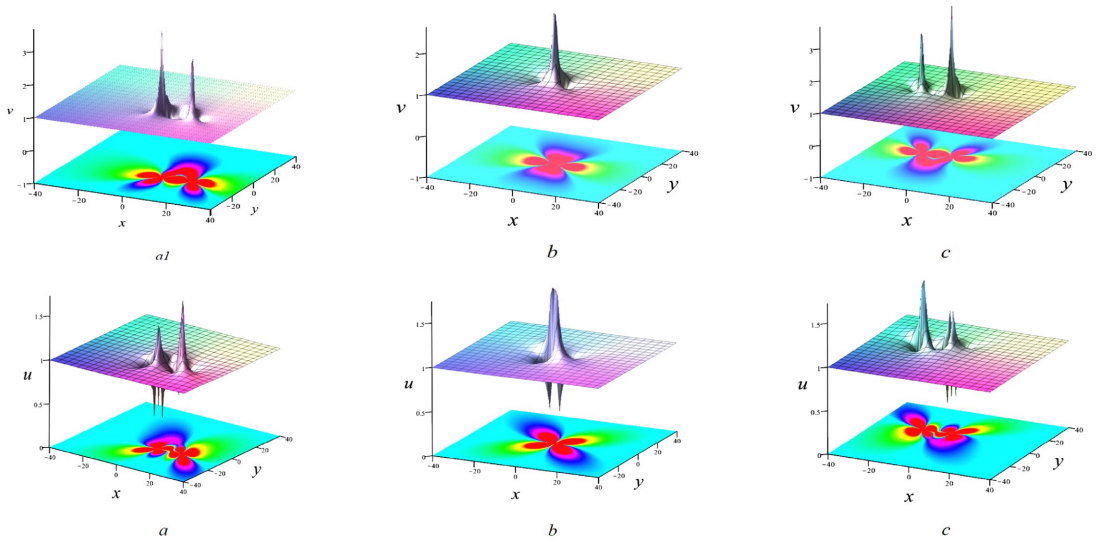

Figure 5. Patial structure diagram of the 2-order lump solution for the KdV equation along with the corresponding projection density plot, (a) - (c) show the spatial profiles of the lump solution in $t = 2.5$, $t = 0$, $t = -2.5$.

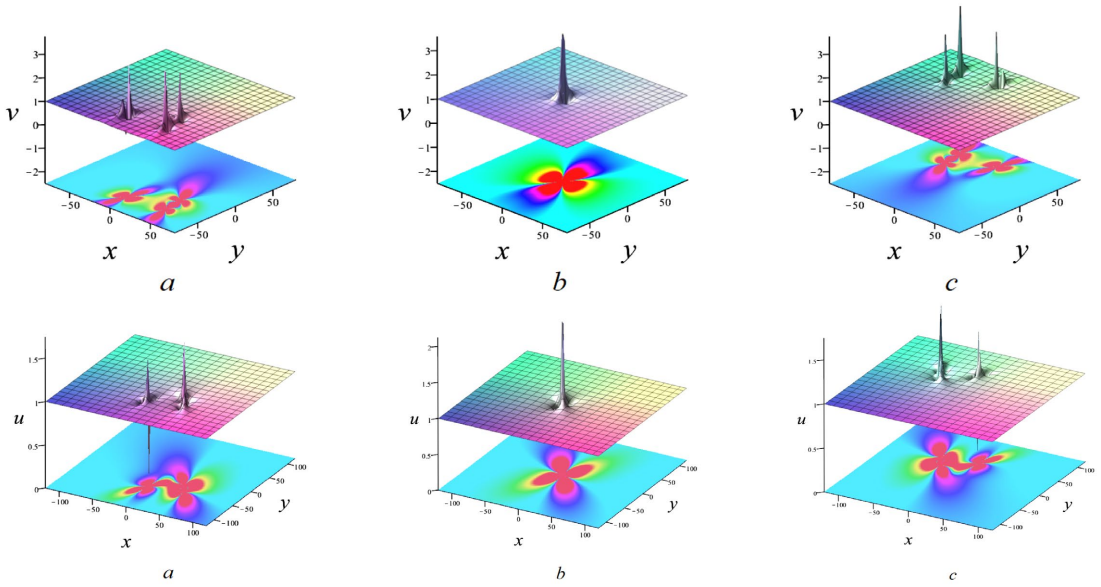

Figure 6. Patial structure diagram of the 3-order lump solution for the KdV equation along with the corresponding projection density plot, (a) - (c) show the spatial profiles of the lump solution in: $t = 5$, $t = 0$, $t = -5$.

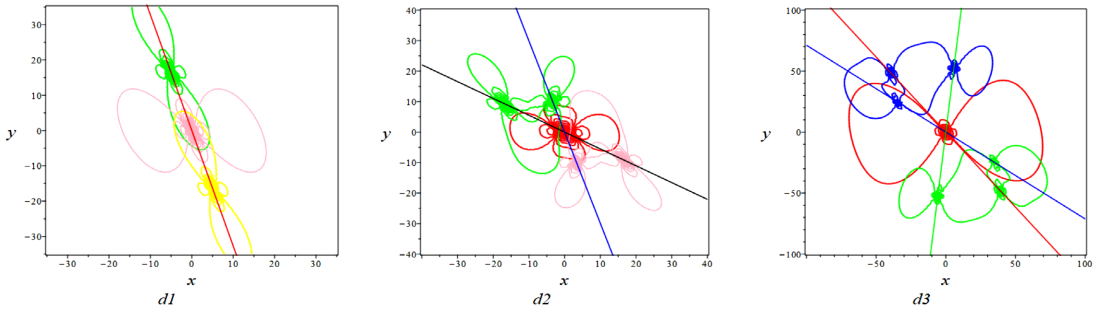

Figure 7. The trajectory of the L-order lump ($L = 1, 2, 3$).

4. Hybridization and Trajectory between 1-Order Lump and *M*-Order Solution

Based on the known *N*-soliton solutions of the KdV equation, the form of 1-lump solution interacting with *N*-soliton solutions can be derived. This section focuses on investigating the trajectory equation of the lump after interaction and the changes in its phase shift. Drawing on the methodology previously employed for studying lump solutions, we let $N=2+m$, $\mathrm{e}^{\sigma_i}=1\left(i=1,2\right)$, $k_1\to 0$, $k_2\to 0$, can obtain:

$$f_{2+m}=\sum_{\nu=0,1}\left(\left(\delta_1+\sum_{s\geq 2}^{2+m}\nu_s G_{1s}\right)\left(\delta_2+\sum_{r\geq 2}^{2+m}\nu_r G_{2r}\right)+P_{12}\right)\exp\left(\sum_{i=2}^{2+m}\nu_i\zeta_i+\sum_{2\leq i<j}^{(2+m)}A_{ij}\nu_i\nu_j\right) \tag{22}$$

where $\nu_2=0, m>0, \delta_1, \delta_2, P_{12}$ refer to (13)

$$G_{ir}=\frac{2k_r q_i q_r\left(q_i+q_r\right)}{-k_r^2 q_r^2 q_i+u_0\left(q_i-q_r\right)^2} \tag{23}$$

By substituting (22) into (2), we can obtain a 1-order lump and *m*-order solution, when $m=1,2$, we can obtain:

$$f_3=\delta_1\delta_2+P_{12}+\left(G_{13}G_{23}+G_{13}\delta_2+G_{23}\delta_1+\delta_1\delta_2+P_{12}\right)\mathrm{e}^{\zeta_3} \tag{24}$$

$$\begin{aligned} f_4=&\delta_1\delta_2+P_{12}+\left(\left(G_{13}+\delta_1\right)+\left(G_{23}+\delta_2\right)+P_{12}\right)\mathrm{e}^{\zeta_3}\\ &+\left(\left(G_{14}+\delta_1\right)+\left(G_{24}+\delta_2\right)+P_{12}\right)\mathrm{e}^{\zeta_4}\\ &+\left(\left(\left(G_{13}+G_{14}+\delta_1\right)+\left(G_{23}+G_{24}+\delta_2\right)+P_{12}\right)\right)\mathrm{e}^{\zeta_3+\zeta_4+A_{34}} \end{aligned} \tag{25}$$

They represent the interaction solutions between 1-lump and 1-soliton, as well as between 1-lump and 2-solitons, respectively.

Theorem 3 The trajectories of this peak before and after the collision between 1-lump and *m*-order solition are as follows:

$$\begin{aligned} x_{-\inf}&=\frac{3t\left(q_1q_2v_0+q_1u_0+q_2u_0\right)}{q_1q_2}+\sum_{i=3}^{2+m}g_{-\inf}\left(\varepsilon_i\right)\psi_i,\\ y_{-\inf}&=-\frac{3tu_0}{q_1q_2}+\sum_{i=3}^{2+m}g_{-\inf}\left(\varepsilon_i\right)\omega_i\\ x_{\inf}&=\frac{3t\left(q_1q_2v_0+q_1u_0+q_2u_0\right)}{q_1q_2}+\sum_{i=3}^{2+m}g_{\inf}\left(\varepsilon_i\right)\psi_i,\\ y_{\inf}&=-\frac{3tu_0}{q_1q_2}+\sum_{i=3}^{2+m}g_{\inf}\left(\varepsilon_i\right)\omega_i \end{aligned} \tag{26}$$

where

$$g_{-\inf}=\begin{cases}1, & x<0\\ 0, & x\geq 0\end{cases};\quad g_{\inf}=\begin{cases}0, & x\leq 0\\ 1, & x>0,\end{cases} \tag{27}$$

$$\begin{aligned} \psi_i&=\frac{2k_iq_1q_2q_i\left(k_i^2q_i^3-q_1q_2u_0-q_1q_iu_0-q_2q_iu_0+3q_i^2u_0\right)}{\left(k_i^2q_2q_i^2-u_0\left(q_2-q_i\right)^2\right)\left(k_i^2q_1q_i^2-u_0\left(q_1-q_i\right)^2\right)}\\ \omega_i&=\frac{2k_iq_i^2\left(k_i^2q_1q_2q_i+3q_1q_2u_0-q_1q_iu_0-q_2q_iu_0-q_i^2u_0\right)}{\left(k_i^2q_2q_i^2-u_0\left(q_2-q_i\right)^2\right)\left(k_i^2q_1q_i^2-u_0\left(q_1-q_i\right)^2\right)} \end{aligned} \tag{28}$$

and the $(x-, y-)$ and $(x+, y+)$ represent the trajectories before and after the collision, respectively. The phase difference is

$$\Delta D = \sum_{i=3}^{2+m} sign(\varepsilon_i) \frac{(\omega_i(\alpha_1+\alpha_2)+\psi_i)u_0 + v_0\alpha_1\alpha_2\omega_i}{(\alpha_1+\alpha_2)u_0 + \alpha_1\alpha_2 v_0} \tag{29}$$

Proof Similar to Theorem 2, considering the trajectory of the 1-order lump, we impose the following restrictions on x and y:

$$x = \frac{3t(q_1q_2v_0 + q_1u_0 + q_2u_0)}{q_1q_2} + c_1, \quad y = -\frac{3tu_0}{q_1q_2} + c_2 \tag{30}$$

Take (30) into (24)

$$f_3 = \kappa_1\kappa_2 + P_{12} + (G_{13}G_{23} + G_{13}\kappa_2 + G_{23}\kappa_1 + \kappa_1\kappa_2 + P_{12})e^{\varepsilon_3 t + \mu_3} \tag{31}$$

with

$$\begin{aligned} \varepsilon_i &= k_i\left(\frac{3(v_0\alpha_1\alpha_2 + \alpha_1u_0 + \alpha_2u_0) - 3\alpha i u_0}{\alpha_1\alpha_2} - k_i^2 - 3v_0 - \frac{3u_0}{\alpha\alpha_i}\right) \\ \mu_i &= k_i(\alpha_i c_1 + c_1) + \sigma_i \\ \kappa_i &= \alpha_i c_2 + c_1 \end{aligned} \tag{32}$$

The sign of μ_3 yields different trajectory equations, when $\mu_3 > 0$,

$$\begin{aligned} f_3^- &= \kappa_1\kappa_2 + P_{12}, (t \to -\infty) \\ f_3^+ &= G_{13}G_{23} + G_{13}\kappa_2 + G_{23}\kappa_1 + \kappa_1\kappa_2 + P_{12}, (t \to +\infty) \end{aligned} \tag{33}$$

Through (28), we can derive the forms of c_1, c_2 as:

$$c_1 = \frac{q_1q_2x - 3t(q_1q_2v_0 + q_1u_0 + q_2u_0)}{q_1q_2}, \quad c_2 = \frac{q_1q_2y + 3tu_0}{q_1q_2} \tag{34}$$

By substituting c_1 and c_2 into (31), we obtain:

$$\begin{aligned} f_3^- &= \delta_1\delta_2 + P_{12}, \\ f_3^+ &= G_{13}G_{23} + G_{13}\delta_2 + G_{23}\delta_1 + \delta_1\delta_2 + P_{12} \end{aligned} \tag{35}$$

Substituting (31) into $v(x, y, t) = v_0 + 2(\ln f)_{xx}$, similar to the solution procedure for the lump trajectory described previously, we obtain the trajectories of the lump wave before and after collision with the line wave as follows:

$$\begin{aligned} y_{-\inf} &= -\frac{u_0 x_{-\inf}}{(\alpha_1+\alpha_2)u_0 + \alpha_1\alpha_2 v_0} \\ y_{\inf} &= -\frac{\left(x_{\inf} - \frac{2k_3\alpha_1\alpha_2\alpha_3(\alpha_3^3k_3^2 - \alpha_1\alpha_2u_0 - \alpha_1\alpha_3u_0 - \alpha_2\alpha_3u_0 + 3\alpha_3^2u_0)}{(k_3^2\alpha_2\alpha_3^2 - u_0(\alpha_2-\alpha_3)^2)(k_3^2\alpha_1\alpha_3^2 - u_0(\alpha_1-\alpha_3)^2)}\right)u_0}{\alpha_1\alpha_2v_0 + \alpha_1u_0 + \alpha_2u_0} \\ &\quad + \frac{2k_3\alpha_3^2(\alpha_1\alpha_2\alpha_3k_3^2 + 3\alpha_1\alpha_2u_0 - \alpha_1\alpha_3u_0 - \alpha_2\alpha_3u_0 - \alpha_3^2u_0)}{(k_3^2\alpha_2\alpha_3^2 - u_0(\alpha_2-\alpha_3)^2)(k_3^2\alpha_1\alpha_3^2 - u_0(\alpha_1-\alpha_3)^2)} \end{aligned} \tag{36}$$

Clearly, Equation (25) holds for the case of $n = 1$. The phase difference of the lump solution is solved as follows:

$$\begin{aligned}\Delta D &= y_{\inf} - y_{-\inf} \\ &= -\frac{2\alpha_1\left(-k_3^2\alpha_3^3 - 3\alpha_3^2u_0 + u_0\left(\alpha_1+\alpha_2\right)\alpha_3 + \alpha_1\alpha_2u_0\right)\alpha_2\alpha_3u_0k_3}{\left(\left(\alpha_1+\alpha_2\right)u_0 + \alpha_1\alpha_2v_0\right)\left(k_3^2\alpha_2\alpha_3^2 - u_0\left(\alpha_2-\alpha_3\right)^2\right)\left(k_3^2\alpha_1\alpha_3^2 - u_0\left(\alpha_1-\alpha_3\right)^2\right)} \\ &\quad + \frac{2k_3\alpha_3^2\left(\alpha_1\alpha_2\alpha_3k_3^2 + 3\alpha_1\alpha_2u_0 - \alpha_1\alpha_3u_0 - \alpha_2\alpha_3u_0 - \alpha_3^2u_0\right)}{\left(-k_3^2\alpha_2\alpha_3^2 + u_0\left(\alpha_2-\alpha_3\right)^2\right)\left(-k_3^2\alpha_1\alpha_3^2 + u_0\left(\alpha_1-\alpha_3\right)^2\right)} \\ &= \frac{u_0\psi_3}{q_1q_2v_0 + q_1u_0 + q_2u_0} + \omega_3\end{aligned} \tag{37}$$

The case of $\mu_3 < 0$ is roughly the same as the above calculation process, and will not be repeated. Next, let's examine the case when $m = 2$. Combining (24) and (28), f_4 can be transformed into:

$$\begin{aligned}f_4 &= \kappa_1\kappa_2 + P_{12} + \left(G_{13}G_{23} + G_{13}\kappa_2 + G_{23}\kappa_1 + \kappa_1\kappa_2 + P_{12}\right)\mathrm{e}^{\varepsilon_3t+\mu_3} \\ &\quad + \left(G_{14}G_{24} + G_{14}\kappa_2 + G_{24}\kappa_1 + \kappa_1\kappa_2 + P_{12}\right)\mathrm{e}^{\varepsilon_4t+\mu_4} \\ &\quad + \left(\kappa_1\kappa_2 + \left(G_{23}+G_{24}\right)\kappa_1 + \left(G_{13}+G_{14}\right)\kappa_2 + P_{12}\right. \\ &\quad \left. + G_{13}G_{23} + G_{14}G_{23} + G_{13}G_{24} + G_{14}G_{24}\right)\mathrm{e}^{\varepsilon_3t+\varepsilon_4+\mu_3+\mu_4+A_{34}}\end{aligned} \tag{38}$$

The definitions of ε_i and μ_i can be found in (30). There are four possible combinations of positive and negative values for ε_3 and ε_4, but we only consider two of them here.

Case 1: When $\varepsilon_3 > 0$, $\varepsilon_4 > 0$, $t \to \pm\infty$, Equation (36) is changed to

$$\begin{aligned}y_4^- &= \kappa_1\kappa_2 + P_{12} \\ y_4^+ &= \kappa_1\kappa_2 + \left(G_{23}+G_{24}\right)\kappa_1 + \left(G_{13}+G_{14}\right)\kappa_2 + P_{12} \\ &\quad + G_{13}G_{23} + G_{14}G_{23} + G_{13}G_{24} + G_{14}G_{24}\end{aligned} \tag{39}$$

The situation is analogous to that of $n = 1$, we can obtain the trajectory equations of the 1-lump before and after collision:

$$\begin{aligned}x_{-\inf} &= \frac{3t\left(\alpha_1\alpha_2v_0 + \alpha_1u_0 + \alpha_2u_0\right)}{\alpha_1\alpha_2} \\ y_{-\inf} &= -\frac{3tu_0}{\alpha_1\alpha_2} \\ x_{\inf} &= \frac{3t\left(\alpha_1\alpha_2v_0 + \alpha_1u_0 + \alpha_2u_0\right)}{\alpha_1\alpha_2} + \psi_3 + \psi_4 \\ y_{\inf} &= -\frac{3tu_0}{\alpha_1\alpha_2} + \omega_3 + \omega_4\end{aligned} \tag{40}$$

The phase difference is:

$$\Delta D = y_{\inf} - y_{-\inf} = \frac{\left(\left(\omega_3+\omega_4\right)\alpha_1 + \left(\omega_3+\omega_4\right)\alpha_2 + \psi_3 + \psi_4\right)u_0 + v_0\alpha_1\alpha_2\left(\omega_3+\omega_4\right)}{\left(\alpha_1+\alpha_2\right)u_0 + \alpha_1\alpha_2v_0} \tag{41}$$

This case satisfies Theorem 3.

Case 2: When $\varepsilon_3 > 0, \varepsilon_4 < 0$, $t \to \pm\infty$, Equation (36) is changed to

$$\begin{aligned}f_4^- &= G_{13}G_{23} + G_{13}\kappa_2 + G_{23}\kappa_1 + \kappa_1\kappa_2 + P_{12} \\ f_4^+ &= G_{14}G_{24} + G_{14}\kappa_2 + G_{24}\kappa_1 + \kappa_1\kappa_2 + P_{12}\end{aligned} \tag{42}$$

Similarly, through the aforementioned calculation process, we can obtain the trajectory equations after the collision between 1-lump and 2-solutions:

$$\begin{aligned}
x_{-\inf} &= \frac{3t\left(\alpha_1\alpha_2 v_0+\alpha_1 u_0+\alpha_2 u_0\right)}{\alpha_1\alpha_2}+\frac{2k_3\alpha_1\alpha_2\alpha_3\left(\alpha_3^3k_3^2-\alpha_1\alpha_2u_0-\alpha_1\alpha_3u_0-\alpha_2\alpha_3u_0+3\alpha_3^2u_0\right)}{\left(k_3^2\alpha_2\alpha_3^2-u_0\left(\alpha_2-\alpha_3\right)^2\right)\left(k_3^2\alpha_1\alpha_3^2-u_0\left(\alpha_1-\alpha_3\right)^2\right)}\\
y_{-\inf} &= -\frac{3tu_0}{\alpha_1\alpha_2}+\frac{2k_3\alpha_3^2\left(\alpha_1\alpha_2\alpha_3k_3^2+3\alpha_1\alpha_2u_0-\alpha_1\alpha_3u_0-\alpha_2\alpha_3u_0-\alpha_3^2u_0\right)}{\left(k_3^2\alpha_2\alpha_3^2-u_0\left(\alpha_2-\alpha_3\right)^2\right)\left(k_3^2\alpha_1\alpha_3^2-u_0\left(\alpha_1-\alpha_3\right)^2\right)}\\
x_{\inf} &= \frac{3t\left(\alpha_1\alpha_2 v_0+\alpha_1 u_0+\alpha_2 u_0\right)}{\alpha_1\alpha_2}+\frac{2k_4\alpha_1\alpha_2\alpha_4\left(\alpha_4^3k_4^2-\alpha_1\alpha_2u_0-\alpha_1\alpha_4u_0-\alpha_2\alpha_4u_0+3\alpha_4^2u_0\right)}{\left(k_4^2\alpha_2\alpha_4^2-u_0\left(\alpha_2-\alpha_4\right)^2\right)\left(k_4^2\alpha_1\alpha_4^2-u_0\left(\alpha_1-\alpha_4\right)^2\right)}\\
y_{\inf} &= -\frac{3tu_0}{\alpha_1\alpha_2}+\frac{2k_4\alpha_4^2\left(\alpha_1\alpha_2\alpha_4k_4^2+3\alpha_1\alpha_2u_0-\alpha_1\alpha_4u_0-\alpha_2\alpha_4u_0-\alpha_4^2u_0\right)}{\left(k_4^2\alpha_2\alpha_4^2-u_0\left(\alpha_2-\alpha_4\right)^2\right)\left(k_4^2\alpha_1\alpha_4^2-u_0\left(\alpha_1-\alpha_4\right)^2\right)}
\end{aligned} \tag{43}$$

The phase difference is:

$$\Delta D = y_{\inf}-y_{-\inf} = \frac{\left(\left(\omega_3-\omega_4\right)\alpha_1+\left(\omega_3-\omega_4\right)\alpha_2+\psi_3-\psi_4\right)u_0+v_0\alpha_1\alpha_2\left(\omega_3-\omega_4\right)}{\left(\alpha_1+\alpha_2\right)u_0+\alpha_1\alpha_2v_0} \tag{44}$$

This case satisfies Theorem 3. The remaining two cases are similar to the aforementioned proof method, and will not be elaborated here. When $m\geq 3$, by combining (21) and (28), the following expression can be obtained:

$$f_{2+m} = \sum_{\nu=0,1}\left(\left(\kappa_1+\sum_{s\geq 2}^{2+m}\nu_sG_{1s}\right)\left(\kappa_2+\sum_{r\geq 2}^{2+m}\nu_rG_{2r}\right)+P_{12}\right)\exp\left(\sum_{i=2}^{2+m}\nu_i\left(\varepsilon_it+\mu_i\right)+\sum_{2\leq i<j}^{(2+m)}A_{ij}\nu_i\nu_j\right) \tag{45}$$

If assuming $\varepsilon_r,\varepsilon_r\cdots,\varepsilon_l,\varepsilon_n$ are positive, the rest of $\varepsilon_i,\left(i\neq r,s,\cdots,l,n\right)$ are negative. Thus, (41) can be written:

$$\begin{aligned}
f_{2+m}^{-} &= \sum_{\nu=0,1}\left(\left(\kappa_1+\sum_{i\neq r,s,\cdots,l,n}^{2+m}\nu_iG_{1i}\right)\left(\kappa_2+\sum_{i\neq r,s,\cdots,l,n}^{2+m}\nu_jG_{2j}\right)+P_{12}\right)\\
f_{2+m}^{+} &= \sum_{\nu=0,1}\left(\left(\kappa_1+\sum_{i=r,s,\cdots,l,n}^{2+m}\nu_iG_{1i}\right)\left(\kappa_2+\sum_{i=r,s,\cdots,l,n}^{2+m}\nu_jG_{2j}\right)+P_{12}\right)
\end{aligned} \tag{46}$$

By combining (28) with the previous calculation process of m = 1, 2, we can obtain (25) and the phase difference (29). The proof of the theorem is complete. Furthermore, by eliminating the time t in (25), we obtained the trajectory equation of the lump solution before and after collision with the m-order solution, which is

$$\begin{aligned}
y_{-\inf} &= -\frac{u_0}{\left(\alpha_1+\alpha_2\right)u_0+\alpha_1\alpha_2v_0}\left(x_{-\inf}-\sum_{i=3}^{2+m}g_{-\inf}\left(\varepsilon_i\right)\psi_i\right)+\sum_{i=3}^{2+m}g_{-\inf}\left(\varepsilon_i\right)\omega_i\\
y_{\inf} &= -\frac{u_0}{\left(\alpha_1+\alpha_2\right)u_0+\alpha_1\alpha_2v_0}\left(x_{\inf}-\sum_{i=3}^{2+m}g_{\inf}\left(\varepsilon_i\right)\psi_i\right)+\sum_{i=3}^{2+m}g_{\inf}\left(\varepsilon_i\right)\omega_i
\end{aligned} \tag{47}$$

From the trajectory equation, it can be observed that the speed and direction remain unchanged after the collision, but the phase has changed. Next, the three-dimensional images of two examples with $m=1,2$ clearly demonstrate the interaction behavior and motion trajectories among the mixed solutions.

First, we present the 3D images of 1-lump and 1-soliton at three different times, with the following parameter settings: $\alpha_2 = \alpha_1^* = -\frac{4}{5} + \mathrm{I}$, $\alpha_3 = 1$, $k_3 = -1$, $\sigma_3 = 0$, $v_0 = 1$, $u_0 = 1$ From Figure 8, it can be observed that the lump and soliton undergo elastic collision. The peak values and shapes remain unchanged before and after the collision. Substituting the parameters into (45), the trajectory is $y_{-\inf} = -25x$ (red), $y = -25x - \frac{211900}{19001}$ (black) (see Figure 10(a)).

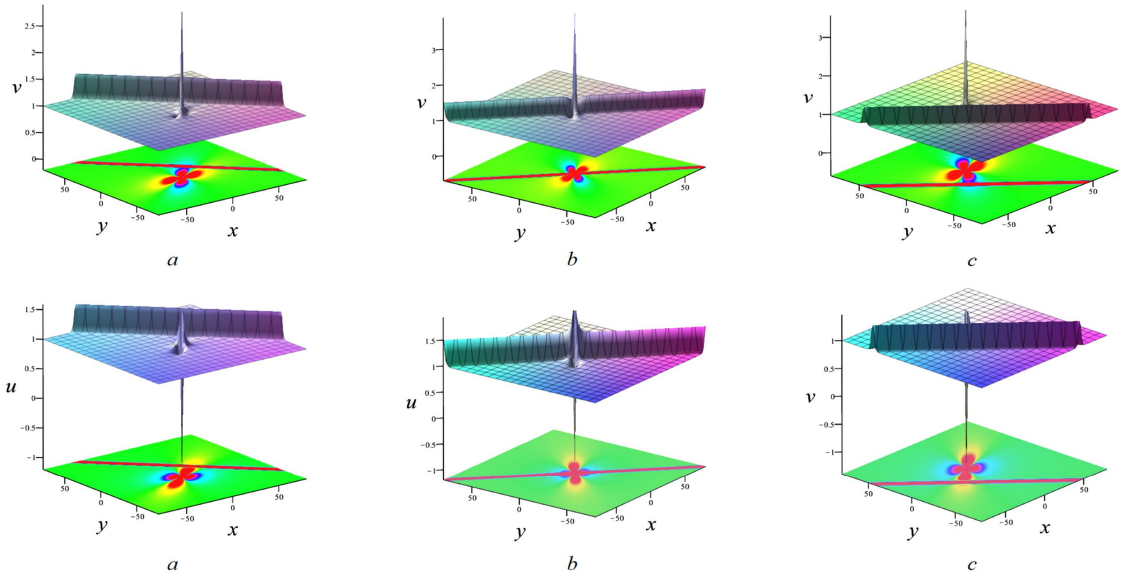

Figure 8. Spatial structure diagram of the 1-order lump and 1-solution for the KdV equation along with the corresponding projection density plot.

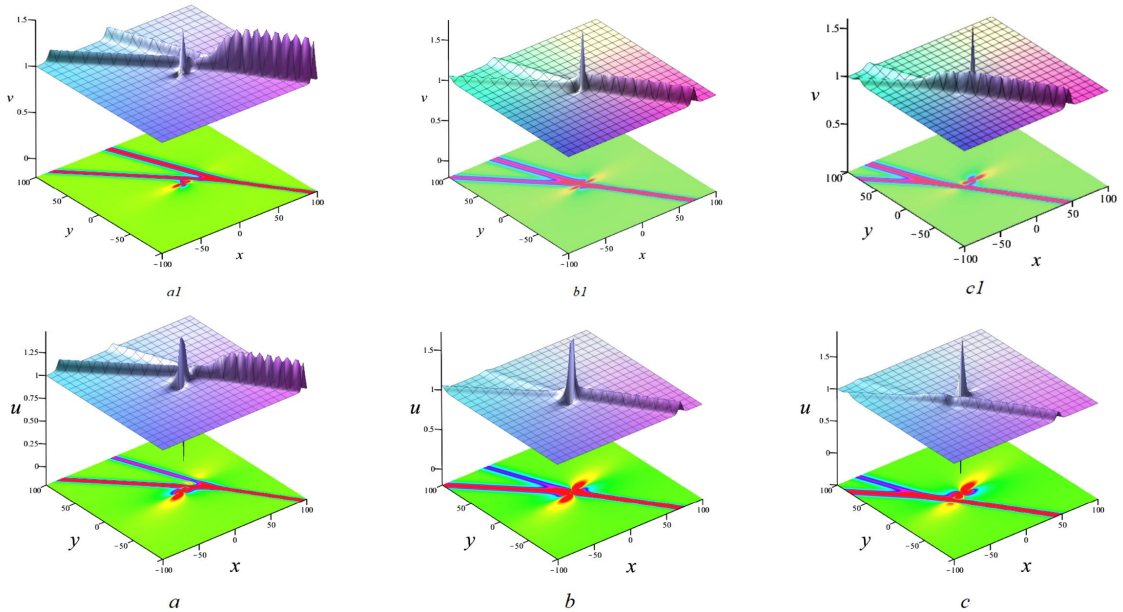

Figure 9. Spatial structure diagram of the 1-order lump and 2-solution for the KdV equation along with the corresponding projection density plot.

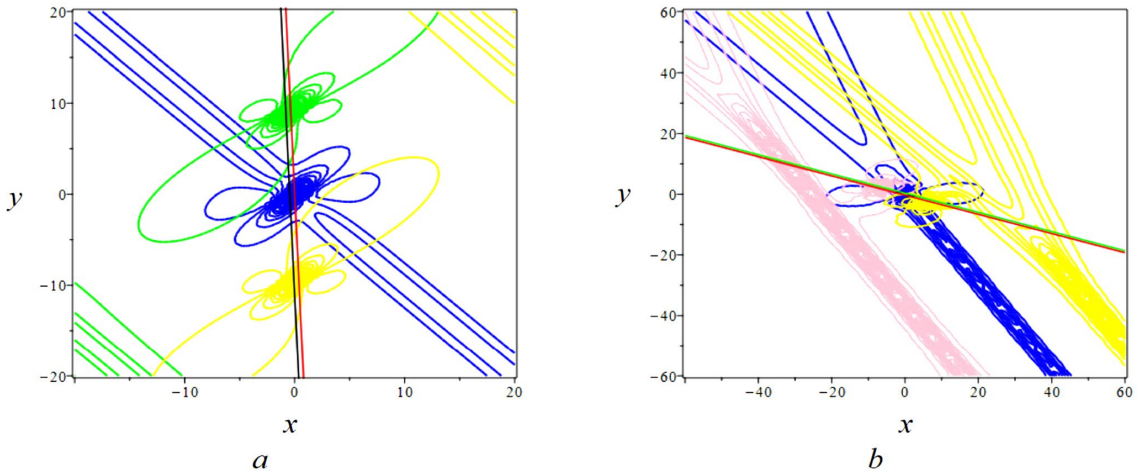

Figure 10. The collision trajectory diagram of lump solutions in the interaction between 1-lump and m-solitons. (a) $m = 1$; (b) $m = 2$.

Next, we present 3D images of 1-lump and 2-solitons at three different time points, with the following parameter settings: $\alpha_2 = \alpha_1^* = \frac{3}{5} - 2$, $\alpha_3 = \frac{2}{5}$, $\alpha_4 = 1$, $k_3 = \frac{1}{2}$, $k_4 = -\frac{1}{2}$, $\sigma_3 = \sigma_4 = 0$, $u_0 = 1$, $v_0 = 1$. The same interaction is also an elastic collision (see **Figure 9**). Substituting the parameters into its trajectory equation is $y_{-\inf} = -\frac{25x}{79} + \frac{85452}{246875}$ (green), $y_{\inf} = -\frac{25x}{79} - \frac{3816800}{12975513}$ (red) (see **Figure 10**).

5. Conclusion

In this paper, the N-solution solutions of the (2 + 1)-dimensional KdV equation are studied to derive various exact solutions. In the first part, by applying conjugate transformations to the parameters in the N-solution solutions, T-order breather solutions are obtained. The quantitative relationships between the parameters determine the positions of the breather solutions when projected onto the xy-plane. In the second part, L-order lump solutions are derived from the N-solution solutions, and the motion trajectories of 1st-, 2nd-, and 3rd-order lumps are analyzed. In the third part, further restrictions on the parameters yield mixed solutions consisting of 1-lump and N-solution solutions. The motion trajectory of the 1-lump before and after collision with the N-solutions is examined. Additionally, the KdV equation possesses many intriguing properties that warrant further investigation, such as the interactions between higher-order breather solutions and higher-order lump solutions.

Acknowledgements

This work has been supported by the National Natural Science Foundation of China (Grant No. 12461047) and the Scientific Research Project of the Hunan Education Department (Grant No. 24B0478).

Conflicts of Interest

The authors declare no conflicts of interest regarding the publication of this paper.

References

[1] Gardner, C.S., Greene, J.M., Kruskal, M.D. and Miura, R.M. (1967) Method for Solving the Korteweg-Devries Equation. *Physical Review Letters*, **19**, 1095-1097. https://doi.org/10.1103/physrevlett.19.1095

[2] Matveev, V.B. and Salle, M.A. (1991) Darboux Transformations and Linear Equations. In: *Springer Series in Nonlinear Dynamics*, Springer, 7-28. https://doi.org/10.1007/978-3-662-00922-2_2

[3] Wahlquist, H.D. and Estabrook, F.B. (1973) Bäcklund Transformation for Solutions of the Korteweg-de Vries Equation. *Physical Review Letters*, **31**, 1386-1390. https://doi.org/10.1103/physrevlett.31.1386

[4] Hirota, R. (1971) Exact Solution of the Korteweg-de Vries Equation for Multiple Collisions of Solitons. *Physical Review Letters*, **27**, 1192-1194. https://doi.org/10.1103/physrevlett.27.1192

[5] Olver, P.J. (1993) Applications of Lie Groups to Differential Equations. Springer Science and Business Media.

[6] Xu, J. and Fan, E.G. (2015) Long-Time Asymptotics for the Fokas-Lenells Equation with Decaying Initial Value Problem: Without Solitons. *Journal of Differential Equations*, **259**, 1098-1148.

[7] Zhao, P. and Fan, E.G. (2020) Finite Gap Integration of the Derivative Nonlinear Schrödinger Equation: A Riemann-Hilbert Method. *Journal of Nonlinear Science*, **30**, 3019-3052.

[8] Tian, S.F. (2017) Initial-Boundary Value Problems for the General Coupled Nonlinear Schrödinger Equation on the Interval via the Fokas Method. *Journal of Differential Equations*, **262**, 506-558. https://doi.org/10.1016/j.jde.2016.09.033

[9] Dai, C.Q., Wang, Y.Y., Tian, Q. and Zhang, J.F. (2012) The Management and Containment of Self-Similar Rogue Waves in the Inhomogeneous Nonlinear Schrödinger Equation. *Annals of Physics*, **327**, 512-521. https://doi.org/10.1016/j.aop.2011.11.016

[10] Deift, P. and Zhou, X. (1993) A Steepest Descent Method for Oscillatory Riemann-Hilbert Problems. Asymptotics for the Mkdv Equation. *The Annals of Mathematics*, **137**, 295-368. https://doi.org/10.2307/2946540

[11] Hirota, R. (2004) The Direct Method in Soliton Theory. Cambridge University Press. https://www.cambridge.org/core/books/direct-method-in-soliton-theory/

[12] Ma, W.X. (2015) Lump Solutions to the Kadomtsev-Petviashvili Equation. *Physics Letters A*, **379**, 1975-1978. https://doi.org/10.1016/j.physleta.2015.06.061

[13] Gandarias, M.L. and Bruzon, M.S. (2011) Some Weak Self-Adjoint Forced KdV Equations. *Journal of Mathematical Physics*, **52**, Article ID: 043516.

[14] Kudryashov, N.A. (2020) Analytical Solutions of the KdV Equation with Variable Coefficients. *Communications in Nonlinear Science and Numerical Simulation*, **91**, Article ID: 105430.

[15] Wang, M.L., Li, X.M. and Zhang, J.H. (2021) Exact Solutions of the KdV Equation via the Exp-Function Method. *Applied Mathematics Letters*, **122**, Article ID: 107494.

[16] Freeman, N.C. and Nimmo, J.J.C. (1983) Soliton Solutions of the Korteweg-de Vries and Kadomtsev-Petviashvili Equations: The Wronskian Technique. *Physics Letters A*, **95**, 1-3. https://doi.org/10.1016/0375-9601(83)90764-8

[17] Ma, W.X., Huang, T.W. and Zhang, Y. (2010) Complexiton Solutions to the Korteweg-de Vries Equation. *Physics Letters A*, **374**, 25-33.

[18] Ma, W.X. and You, Y. (2005) Solving the Korteweg-de Vries Equation by Its Bilinear Form: Wronskian Solutions. *Transactions of the American Mathematical Society*, **357**, 1753-1778. https://doi.org/10.1090/s0002-9947-04-03726-2

[19] Tan, W., Zhang, W. and Zhang, J. (2022) Evolutionary Behavior of Breathers and Interaction Solutions with M-Solitons for (2 + 1)-Dimensional KdV System. *Communications in Nonlinear Science and Numerical Simulation*, **115**, Article ID: 106767.